Reprinted from Biochemistry, 1992, 31.

^1H, ^{13}C, and ^{15}N NMR Backbone Assignments and Secondary Structure of Human Interferon-γ†

Stephan Grzesiek,‡,§ Heinz Döbeli,∥ Reiner Gentz,∥ Gianni Garotta,∥ Alexander M. Labhardt,∥ and Ad Bax*,‡

Laboratory of Chemical Physics, National Institute of Diabetes and Digestive and Kidney Diseases, National Institutes of Health, Bethesda, Maryland 20892, and F. Hoffmann La Roche and Company Ltd., Grenzacherstrasse 124, CH-4002 Basel, Switzerland

Received May 20, 1992

ABSTRACT: ^1H, ^{13}C, and ^{15}N NMR assignments of the protein backbone of human interferon-γ, a homodimer of 31.4 kDa, have been made using the recently introduced three-dimensional (3D) triple-resonance NMR techniques. It is shown that, despite the ~40–50-Hz $^{13}C_\alpha$ and $^1H_\alpha$ line widths of this high molecular weight dimer and the extensive overlap in the $^1H_\alpha$ and $^{13}C_\alpha$ spectral regions, unique sequential assignments can be made on the basis of combined use of the 3D HNCO, HNCA, HN(CO)CA, and HCACO constant-time experiments, the ^{15}N-separated 3D NOESY-HMQC, and the 3D HOHAHA-HMQC experiments. Analysis of the ^{15}N-separated 3D NOESY-HMQC and $^{13}C/^{15}N$-separated four-dimensional (4D) NOESY-HMQC spectra together with the secondary C_α and C_β chemical shifts yielded extensive secondary structure information. The NMR-derived secondary structure essentially confirms results of a recently published low-resolution crystal structure [Ealick et al. (1991) *Science 252*, 698–702], i.e., six helices in the monomer which are mostly α-helical in nature, no β-sheets, a long flexible loop between helices A and B, and a very hydrophobic helix C. The functionally important carboxy terminus, which was not observed in the X-ray study, does not adopt a rigid conformation in solution. A high degree of internal mobility, starting at Pro-123, gives rise to significantly narrower resonance line widths for these carboxy-terminal residues compared to the rest of the protein.

Interferon (IFN)[1] was first discovered in 1957 for its antiviral activity (Isaacs & Lindenmann, 1957). Three functionally related, but structurally different interferons, IFN-α, IFN-β, and IFN-γ, have been found in all mammalian species (Ijzermans & Marquet, 1989). IFN-γ was first described by Wheelock (1965) and is distinctly different from IFN-α and IFN-β, whose genes are located on a different chromosome (Shows et al., 1982) and which have very limited homology to IFN-γ (Ijzermans & Marquet, 1989). IFN-γ exhibits a large number of different biological activities, comprising its antiviral activity [for recent reviews, see Ijzermans and Marquet (1989), Murray (1990), Landolfo and Garotta (1991), and Mosmann et al. (1991)], antitumoral and antimicrobial actions, the activation of macrophages, the enhancement of natural killer cell activity and of T-cell cytotoxicity, and the modulation of the B- and T-cell response where it acts in an antagonistic sense to interleukin-4 (Mosmann et al., 1991) as well as the enhancement of MHC class I and II expression. During the immune response, IFN-γ is produced by activated T-cells and natural killer cells (Nathan et al., 1981; Trinchieri et al., 1984). In contrast to IFN-α and IFN-β, the biological active form of IFN-γ is a dimer (Pestka et al., 1983; Le et al., 1984), and the human IFN-γ receptor has been identified [for a recent review, see Langer and Pestka (1988)].

The coding sequence for the mature human IFN-γ comprises 143 amino acids (Ealick et al., 1991; Samudzi et al., 1991). Crystallographic studies on human IFN-γ (3.5-Å resolution; Ealick et al., 1991) and rabbit IFN-γ (2.7-Å resolution; Samudzi et al., 1991) confirmed the high α-helical content of 60–70% which had been predicted on the basis of ultraviolet circular dichroism (Hogrefe et al., 1989; Arakawa et al., 1987). Both crystal structures show the same overall motif where four of the six helices of one monomer form a cleft that accommodates the last helix of the second monomer. However, the definition of the single helices differs to some extent in the two crystal structures.

Residues at both the N-terminus and the C-terminus are involved in modulating the biological response. Whereas antibodies directed against the N- and C-terminus (Seelig et al., 1988; Johnson et al., 1982) block biological activity, only synthetic peptides comprising the N-terminal region of murine IFN-γ block binding to its receptor in a competitive way (Jarpe & Johnson, 1990). Integrity of the N-terminus is essential for the adaptation of a defined secondary structure (Hogrefe et al., 1989). However, removal of up to 13 amino acids from the C-terminus does not affect the conformation (Arakawa et al., 1986), and natural IFN-γ shows various degrees of C-terminal processing (Rinderknecht et al., 1984). Extensive studies on IFN-γ of various C-terminal lengths have been carried out (De la Maza et al., 1987; Döbeli et al., 1988). It has been shown that the biological activity of IFN-γ is enhanced when a limited number of C-terminal residues are removed (Döbeli et al., 1988).

In this study, we report the NMR ^1H, ^{15}N, and ^{13}C backbone resonance assignments and the secondary structure of recombinant human IFN-$\gamma\Delta$10, a form of IFN-γ which lacks

† This work was supported by the Intramural AIDS Anti-viral Program of the Office of the Director of the National Institutes of Health.
* To whom correspondence should be addressed.
‡ National Institutes of Health.
§ On leave from F. Hoffmann La Roche, Basel, Switzerland.
∥ F. Hoffmann La Roche Ltd.
[1] Abbreviations: IFN, interferon; IFN-$\gamma\Delta$10, recombinant human interferon-γ lacking the last 10 amino acids and comprising one additional N-terminal methionine; NMR, nuclear magnetic resonance; NOE, nuclear Overhauser effect; NOESY, nuclear Overhauser enhancement spectroscopy; HMQC, heteronuclear multiple-quantum coherence; 3D, three dimensional; 4D, four dimensional.

0006-2960/92/0431-8180$03.00/0

its last 10 amino acids and has a C-terminal length of maximal biological activity. Our NMR study relies on combined use of conventional 3D ^{15}N-separated NOESY experiments (Marion et al., 1989c; Zuiderweg & Fesik, 1989) and the newer triple-resonance 3D and 4D NMR techniques (Ikura et al., 1990a; Kay et al., 1990a,b). To the best of our knowledge, IFN-γΔ10 with its dimeric molecular mass of 31.4 kDa is the largest protein complex for which complete backbone assignments have been made.

EXPERIMENTAL PROCEDURES

Sample Preparation. Recombinant human IFN-γΔ10 was expressed in 4 L of an *Escherichia coli* culture harboring the plasmid pDMI.1 (Certa et al., 1986) and the expression plasmid pIFNγΔ10 (Döbeli et al., 1988). Cells were grown in M9 minimal medium using 0.15% glucose and 0.1% NH_4Cl as the only carbon and nitrogen source, respectively. Induction of expression was achieved by the addition of 1 mM isopropyl β-D-thiogalactopyranoside at OD_{600nm} = 0.5, and the cells were harvested after an additional period of 4 h.

Cells were separated from the fermentation broth by centrifugation and resuspended in 200 mL of 0.15 M sodium borate, pH 8. Cell disintegration was performed with a Rannie high-pressure homogenizer; IFN-γ remains as a refractory body in the pellet. This pellet is washed twice with 200 mL of 0.15 M sodium borate, pH 8, and then solubilized with 6 M guanidine·HCl and 0.1 M sodium phosphate, pH 7. The further purification and refolding process is as described by Döbeli et al. (1988), comprising centrifugation, silica gel batch adsorption, a phenyl sepharose CL-4B column, a Fractogel TSK CM-650 (M) column, and a Sephacryl S-300 (instead of Sephadex G-50) column. Total yield was ~30 mg.

The amount of incorporated isotopes was measured by mass spectrometry. The average mass of the (monomeric) unlabeled IFN-γ was 15 702.5 ± 2 (theoretical value 15 704.9). For the sample with high levels of ^{13}C and ^{15}N incorporation, the mass was 16 570.3 ± 2 (theoretical value 16 572), indicating that incorporation of the ^{13}C and ^{15}N isotopes was virtually complete.

The recombinant IFN-γΔ10 construct comprises one additional N-terminal Met, resulting in a total length of 134 amino acids for the IFN-γ monomer and a total molecular mass of 31.4 kDa for the dimer. Numbering throughout this paper starts at this N-terminal Met, so that the natural human IFN-γ starts at residue number 2. Three batches of labeled material were prepared: one uniformly labeled to >95% with ^{15}N, a second accidentally labeled to only 50% with ^{15}N and >95% ^{13}C, and the last with >98% ^{15}N and >98% ^{13}C labeling. For NMR spectroscopy, samples were exchanged into 20 mM potassium phosphate, 20 mM NaCl, 0.5 mM NaN_3, and 90% H_2O/10% D_2O or 100% D_2O, pH/pD* 6.2. For all samples, the IFN-γ concentration was approximately 1.4 mM (monomer).

NMR Spectroscopy. All NMR experiments were performed on a Bruker 600-MHz AMX spectrometer equipped with a three-channel NMR interface, a triple-resonance ^{1}H/^{15}N/^{13}C probe, and no further modifications. Because of the limited stability of the sample, a temperature of only 27 °C was used throughout. Except for the 4D ^{15}N/^{13}C-separated NOESY experiment, all triple-resonance experiments were performed with the 50% ^{15}N and >95% ^{13}C material, resulting in an effective monomer concentration of only 0.7 mM. Unless noted otherwise, water concentrations were 90% H_2O/10% D_2O.

3D HNCO, HNCA, and HN(CO)CA spectra were recorded with pulse sequences described earlier, using constant-time evolution for the ^{15}N nucleus (Grzesiek & Bax, 1992a). The number of complex points and acquisition times were as follows: CT-HNCO, ^{15}N (F_1) 32, 24 ms, ^{13}CO (F_2) 64, 34.5 ms, ^{1}H (F_3) 512, 55.3 ms (64 scans per hypercomplex t_1,t_2 increment); CT-HNCA, ^{15}N (F_1) 32, 22.4 ms, ^{13}Cα (F_2) 48, 10 ms, ^{1}H (F_3) 512, 55.3 ms (256 scans per hypercomplex t_1,t_2 increment); CT-HN(CO)CA, ^{15}N (F_1) 32, 19.8 ms, ^{13}Cα (F_2) 46, 9.6 ms, ^{1}H (F_3) 512, 55.3 ms (128 scans per hypercomplex t_1,t_2 increment). HCACO and HCCH-COSY experiments were recorded on the D_2O sample using constant-time evolution in the aliphatic ^{13}C dimension (Powers et al., 1991; Ikura et al., 1991) with the following numbers of complex points and acquisition times: CT-HCACO, ^{13}CO (F_1) 64, 28 ms, $^{13}C_\alpha$ (F_2) 32, 6.4 ms, ^{1}H (F_3) 256, 53.2 ms (128 scans per hypercomplex t_1,t_2 increment); CT-HCCH-COSY, ^{1}H (F_1) 64, 14.7 ms, ^{13}C (F_2) 32, 7.0 ms, ^{1}H (F_3) 256, 53.2 ms (64 scans per hypercomplex t_1,t_2 increment). A ^{15}N-separated 3D NOESY was recorded using presaturation of the H_2O resonance with a 40-Hz rf field during the delay between scans and during the NOE mixing period. The following numbers of complex data points and acquisition times were used: ^{1}H (F_1) 128, 19.2 ms, ^{15}N (F_2) 32, 24 ms, ^{1}H (F_3) 384, 54.5 ms (64 scans per hypercomplex t_1,t_2 increment). A ^{13}C/^{15}N-separated 4D NOESY was recorded with a 60-ms mixing time, using the pulse sequence described by Kay et al. (1990) and using a 10-Hz rf field to presaturate the H_2O resonance during the delay between scans and a "soft–hard" read pulse (Sklenar & Bax, 1987b) at the end of the NOESY mixing period to further suppress the H_2O resonance. The following numbers of complex data points and acquisition times were used: ^{1}H (F_1) 64, 12.8 ms, ^{13}C (F_2) 8, 2.65 ms, ^{15}N (F_3) 16, 12.8 ms, ^{1}H (F_4) 384, 41 ms (64 scans for each set of t_1, t_2, t_3 values). A ^{15}N-separated 3D proton–proton HOHAHA (Marion et al., 1989a) was recorded with a 35-ms mixing period using the DIPSI-2 mixing scheme (Shaka et al., 1988) and the following numbers of data points and acquisition times: ^{1}H (F_1) 100, 20 ms, ^{15}N (F_2) 32, 24 ms, ^{1}H (F_3) 512, 55.3 ms (64 scans per hypercomplex t_1,t_2 increment). The 35-ms mixing period was followed by a 17-ms NOE period (Marion et al., 1989a) to offset the positive NOE occurring during isotropic mixing. A 2D ^{15}N–^{1}H HSQC correlation (Bodenhausen & Ruben, 1980; Bax et al., 1990) with a 1-ms water suppression purge pulse at the end of the first INEPT transfer (Messerle et al., 1989) was recorded on the >95% ^{15}N-labeled sample, using the following numbers of complex data points and acquisition times: ^{15}N (F_1) 128, 64 ms, ^{1}H (F_2) 512, 42 ms (32 scans per complex t_1 increment). Slowly exchanging amide protons were identified by recording one ^{15}N–^{1}H HSQC immediately after exchanging H_2O against D_2O, by repeated microdialysis at 5–10 °C over a period of 23 h, and by recording another spectrum of the same sample 9 months later. Finally, a 2D ^{1}H–^{13}C HMQC correlation spectrum was recorded on the D_2O sample with the following numbers of complex data points and acquisition times: ^{13}C (F_1) 320, 30.9 ms, ^{1}H (F_2) 384, 53 ms (32 scans per complex t_1 increment).

Quadrature detection in all indirectly detected dimensions was obtained by using the States-TPPI acquisition scheme (Marion et al., 1989b). Spectra were processed on Sun Sparc workstations using in-house routines for Fourier transformation and linear prediction in the heavily truncated indirect dimensions (Kay et al., 1989) together with commercially available software (NMR2, New Methods Research, Inc., Syracuse, NY). For the constant-time evolution periods, the

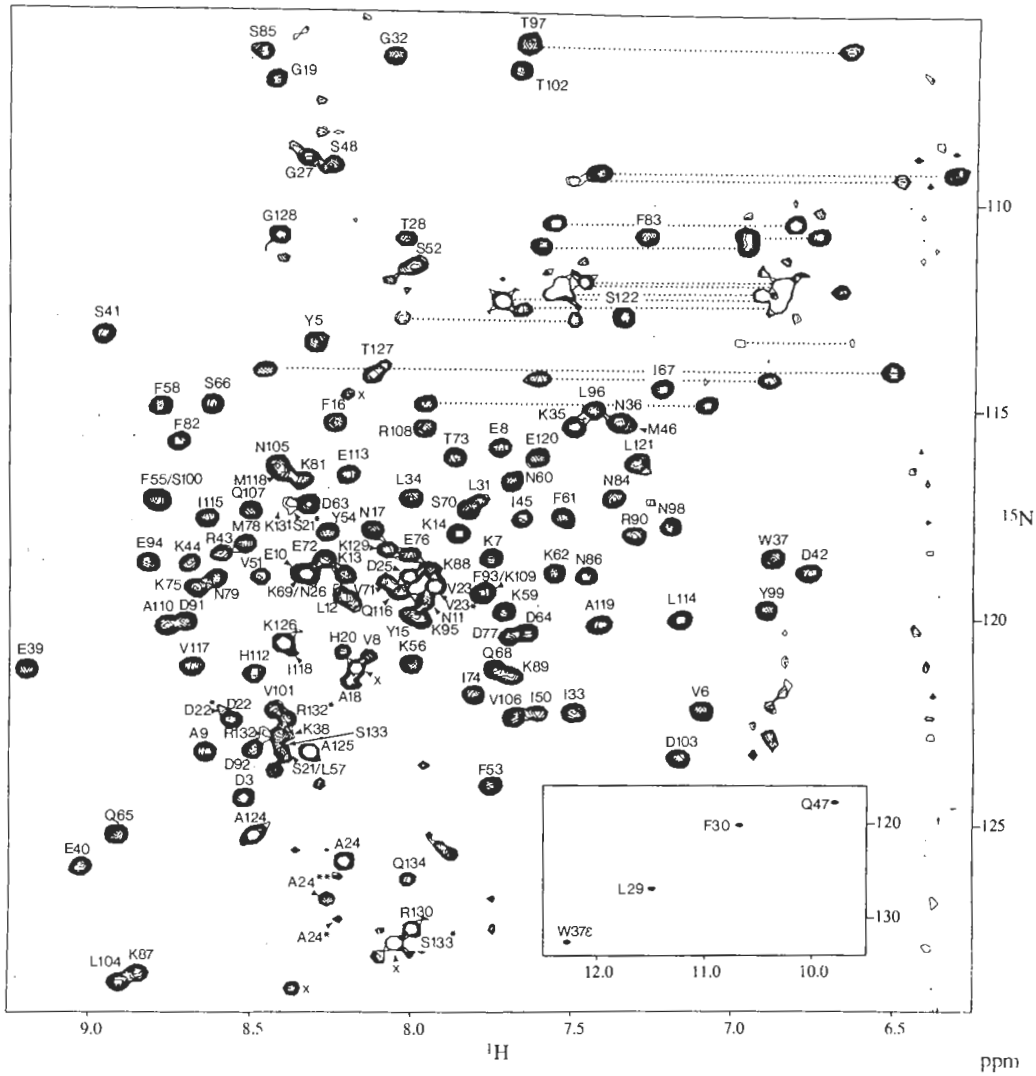

FIGURE 1: Resolution-enhanced 2D ^{1}H–^{15}N HSQC spectrum of IFN-γΔ10, labeled uniformly with ^{15}N (>95%), recorded at 600-MHz ^{1}H frequency. Cross peaks connected by dotted lines correspond to Gln and Asn side chain NH_2 groups. Cross peaks marked "x" were only observed in the ^{15}N (>95%)-labeled sample and not in the ^{15}N/^{13}C-labeled samples. R132* and S133* correspond to protein that terminates at S133. Asterisks for residues S21–D25 correspond to a minor conformer.

"mirror image trick" in linear prediction (Zhu & Bax, 1990) was used throughout. For spectra recorded on H_2O samples, water suppression on the time domain data was achieved by subtracting a fitted fourth-order polynomial from the FID. Analysis of the processed spectra and peak picking was carried out using the in-house programs CAPP and PIPP (Garrett et al., 1991).

RESULTS AND DISCUSSION

2D Experiments. Figure 1 shows a 2D ^{15}N–^{1}H HSQC spectrum of uniformly ^{15}N-labeled IFN-γΔ10. On average, the resonance line widths of the backbone amide ^{15}N nuclei that do not experience high degrees of internal mobility are in the 15–20-Hz range, as determined from the ^{15}N line width in a HSQC ^{1}H–^{15}N correlation spectrum recorded with a long t_1 acquisition period, no digital filtering, and extensive zero filling in the t_1 dimension. Line widths for the amide protons, as determined from the transverse relaxation time measured using a 1–1 spin echo experiment (Sklenar & Bax, 1987a), are ~25 Hz. Although the dispersion of the amide ^{1}H frequencies is rather poor, as expected for this highly α-helical protein (~70% from the 3.5-Å crystal structure; Ealick et al., 1991), the dispersion in the ^{15}N dimension is sufficient to resolve most of the amide signals. However, some regions of substantial overlap remain, particularly around 119 ppm ^{15}N and 7.9–8.4 ppm ^{1}H as well as between 122 and 124 ppm ^{15}N and 8.3–8.5 ppm ^{1}H, where in some cases three correlations have indistinguishable positions (e.g., E10, N26, K69). Although all those degeneracies can be resolved by recursion to the HNCO experiment (Table II), they cause serious problems in the sequential assignment procedure, especially considering that for some of these amides even the C_α frequencies overlap (e.g., E10, K69).

Natural IFN-γ is an inhomogeneous mixture with a high variability in the amount of glycosylation and in the length of the C-terminus (Rinderknecht et al., 1984; Pan et al., 1987). More recently, Curling et al. (1990) showed that recombinant IFN-γ, expressed in eukaryotic cells, is also heterogeneous in its C-terminal length. In all likelihood this is caused by the fact that the C-terminus, with its highly conserved KRKR quartet (Lortat-Jacob & Grimaud, 1991), contains a high number of potential proteolytic cleavage sites (Döbeli et al., 1988). Although our preparations were derived from *E. coli* cell cultures, in all three samples at least two different chain lengths of the C-terminus of IFN-γΔ10 could be identified: one full chain component extending to Q134 and a second component stopping at S133*. This second component could be traced back to R132* and probably coincides at K131 with

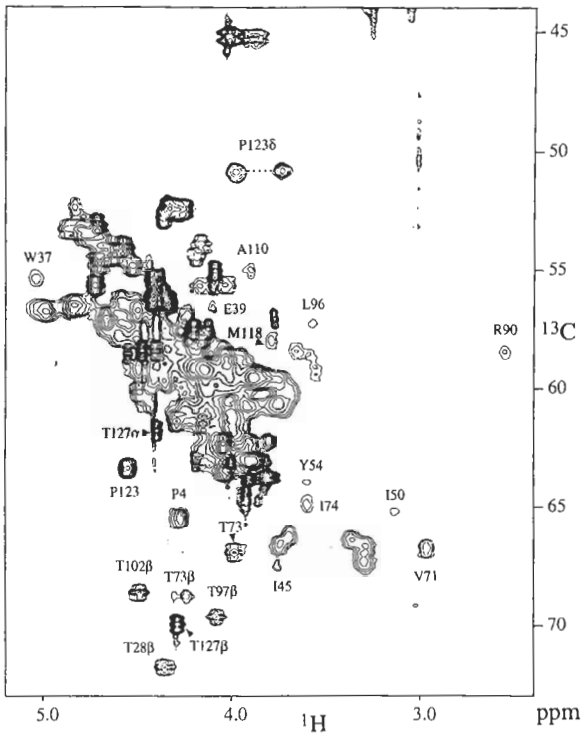

FIGURE 2: H_α–C_α region of the resolution-enhanced 2D ^1H–^{13}C HMQC correlation spectrum of IFN-γΔ10 in D_2O, labeled uniformly with ^{15}N (50%) and ^{13}C (>95%), recorded at 600-MHz ^1H frequency. Only nonoverlapping correlations have been labeled.

the full chain component. Over a period of 9 months a gradual increase of the intensity of the S133* cross peak and a concomitant loss in intensity of Q134 were observed, which is attributed to still ongoing proteolysis in the NMR sample. Furthermore, in the >95% ^{15}N-labeled sample (but not in the other two doubly labeled samples), several other resonances reminiscent of C-terminal residues of other C-terminal variants of IFN-γ were observed.

In all three samples a second type of heterogeneity was observed for the loop region between H20 and D25. This heterogeneity consists of a main fraction (sequentially connected) of about 75% relative intensity, labeled H20, S21, D22, V23, A24, and D25 (Figure 1, Table II), and a second fraction (also sequentially connected) consisting of H20*, S21*, D22*, V23*, A24*, and D25* with 25% relative intensity, respectively. Within this minor fraction there is evidence of further heterogeneity, as evidenced by very weak ^1H–^{15}N correlations in the vicinity of the correlations of the minor component (see, for example, the correlation marked A24** in the vicinity of F_1/F_2 = 127/8.2 ppm in Figure 1) that show identical NOE patterns in the 3D ^{15}N-separated NOESY spectrum. The relative intensities of the A24* and A24** correlations vary for the three samples from a 1:2 ratio (^{15}N-labeled sample) to a 3:1 ratio (50% ^{15}N- and >95% ^{13}C-labeled sample). While the NOE patterns between the amide protons of those minor fractions and aliphatic protons are virtually identical to those observed for the main fraction, as judged from the 4D $^{13}C/^{15}N$-separated NOESY, the reason for this heterogeneity in the amide ^1H and ^{15}N frequencies remains unclear.

Figure 2 shows the H_α–C_α part of a 2D ^1H–^{13}C HMQC correlation spectrum and clearly illustrates the wide range of ^1H–^{13}C cross peak intensities. Residues with extensive internal mobility, such as found near the C-terminus and in several of the loop regions, give rise to relatively narrow line widths and correspondingly strong correlations in the 2D spectrum. Residues in well-ordered regions of secondary structure have H_α line widths of 45–55 Hz and C_α line widths of 35–45 Hz, and these residues show very weak correlations in the 2D spectrum. It is therefore not surprising that in all the proton–carbon correlation experiments, such as the HCACO or the HCCH-COSY experiments, the intensities of resonances in the flexible parts are up to two orders of magnitude larger than for correlations from the more rigid parts of the protein. This large variation in intensities leads to the obliteration of some of the weaker correlations by small truncation artifacts or t_1 noise ridges associated with the very strong resonances.

Assignment Procedure. The recently proposed triple-resonance experiments form the basis for the sequential backbone assignment of IFN-γ. However, because of the high molecular weight and the limited thermal stability of the IFN-γ dimer, only the most sensitive of these experiments, i.e., HNCO, HN(CO)CA, HCACO, and HNCA, yielded useful data, after these experiments were optimized for high molecular weight proteins (Grzesiek & Bax, 1992a). The results of the two ^{15}N-separated 3D experiments, the ^{15}N-NOESY and the ^{15}N-HOHAHA, were used in addition to establish intraresidue connectivities from the amide ^1H_N and ^{15}N to the $^1H_\alpha$ proton. The HCCH-COSY experiment (Ikura et al., 1991) was used to connect the H_α–C_α pair with the H_β–C_β resonances. The C_α–C_β shifts are quite characteristic for the type of amino acid residue involved, and this information yielded unambiguous type assignments for several of the Thr, Ser, and Ala residues. The characteristic C_α shift of glycine residues also identified all of these residues. For many other residues, the C_α–C_β shifts limit the number of possible side chain types.

Cross sections taken through the 3D HNCO, HNCA, and HCACO spectra are shown in Figure 3 and illustrate the quality of the data obtained with these experiments. The ^1H–^{13}CO cross section through the HNCO spectrum has been taken at a ^{15}N chemical shift of 118.9 ppm, perpendicular to a region with substantial overlap in the 2D ^1H–^{15}N correlation spectrum (Figure 1). Clearly, the high degree of dispersion in the ^{13}CO dimension effectively removes these degeneracies in the HNCO spectrum. For example, the degenerate E10, N26, and K69 ^1H–^{15}N correlations now appear as three well-separated resonances. However, the degeneracy problem is not resolved in the HNCA spectrum (Figure 3B), where E10 and K69 also have degenerate C_α frequencies. The correlation for N26 is not observed in this figure because, unlike the HNCO spectrum, the HNCA spectrum was recorded with presaturation of the water resonance, obliterating the amide proton of N26 which exchanges rapidly with solvent protons. Figure 3B also shows several H_i–N_i–$C_{\alpha,i-1}$ connectivities, resulting through the $^2J_{NC\alpha}$ coupling. These connectivities, marked by asterisks, were used together with the results of the HN(CO)CA experiment (Grzesiek & Bax, 1992a) to correlate each ^1H–^{15}N pair to its preceding C_α resonance.

As mentioned above, IFN-γ shows a very wide range of H_α and C_α line widths and the majority of the residues with low degrees of internal mobility having values of 50 and 40 Hz, respectively. Together with the poor dispersion in the H_α and C_α frequencies, this makes the interpretation of H_α- and C_α-separated experiments very difficult. As an example, one slice of the HCACO experiment, connecting H_α, C_α, and its attached carbonyl, is shown for the $^{13}C_\alpha$ frequency of 59.1 ppm (Figure 3C). In particular, the 20 lysine H_α–C_α correlations in IFN-γΔ10 are all subject to severe overlap. The previously mentioned degeneracy of the E10 and K69 $^{13}C_\alpha$ frequencies is dispersed in the HCACO spectrum by

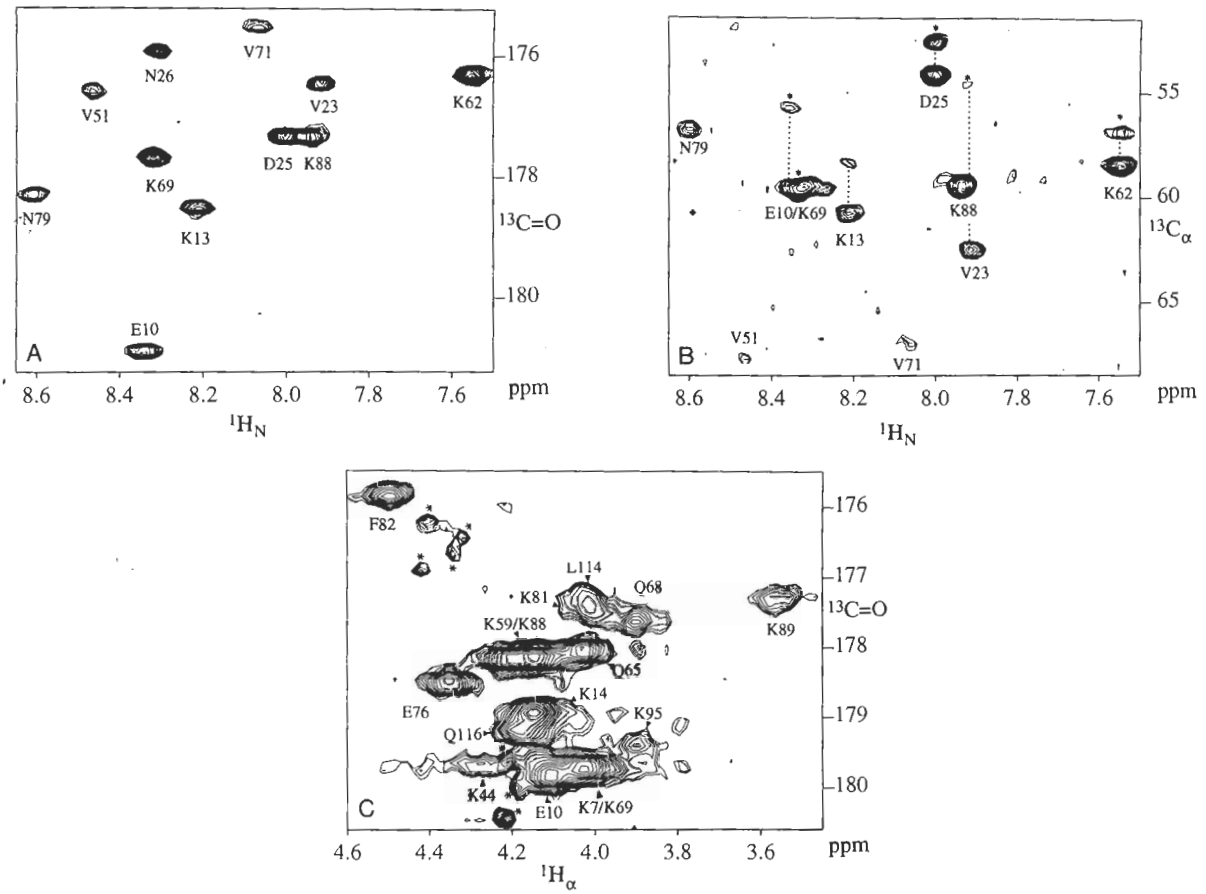

FIGURE 3: Cross sections through several of the triple-resonance spectra of IFN-γΔ10. (A) A $^{1}H_N$–^{13}CO slice of the HNCO spectrum, taken at a ^{15}N chemical shift of 118.9 ppm. (B) A $^{1}H_N$–$^{13}C_\alpha$ slice of the HNCA spectrum, taken at the same ^{15}N chemical shift. Correlations from the amide to the C_α of its preceding amino acid are marked by asterisks. (C) A $^{1}H_\alpha$–^{13}CO cross section through the HCACO spectrum, taken at a $^{13}C_\alpha$ shift of 59.1 ppm. Artifacts from t_1 noise and truncation, associated with the very intense resonances of mobile residues in distant parts of the spectrum, are marked by asterisks.

their slightly different H_α and carbonyl shifts.

Figure 3C also illustrates one of the problems caused by the wide range of different line widths and subsequent resonance intensities in the HCACO spectrum: resonances marked by asterisks are the result of t_1 noise and truncation associated with the sharp and intense resonances in distant parts of the HCACO spectrum.

As has been pointed out before (Ikura et al., 1990a), the sequential backbone assignment procedure using 3D triple-resonance experiments encounters an ambiguity whenever two or more pairs of $^{1}H_\alpha$–$^{13}C_\alpha$ correlations (or of $^{1}H_N$–^{15}N correlations) have frequencies that are indistinguishable at the resolution obtained in the 3D spectra. Note that, in contrast to inferences in recent literature (Kay et al., 1991; Boucher et al., 1992), this type of ambiguity cannot be resolved by increasing the dimensionality of the NMR spectrum to 4D. One elegant solution that does work for resolving the H_α–C_α ambiguity is an experiment that correlates the ^{1}H–^{15}N pair with the intraresidue carbonyl resonance (Clubb et al., 1992). However, this experiment is considerably lower in sensitivity than the HNCA experiment and for this reason not applicable to IFN-γ. A second way to remove the ambiguities relies on determining the amino acid type of the residue preceding each amide via a multistep relay procedure (Grzesiek & Bax, 1992b). However, this technique had not yet been developed at the time the assignment was completed and will therefore not be described here. In the present study, the degeneracy in the H_α–C_α spectrum was resolved by resorting to the 3D ^{15}N-separated and the 4D $^{15}N/^{13}C$-separated NOESY experiments. Below, this hybrid assignment strategy is discussed in some more detail.

Because of its high sensitivity and low degree of resonance overlap, the HNCO experiment is chosen as a starting point to go from one amino acid to its predecessor. The carbonyl frequency of such an HNCO cross peak together with the C_α frequency of the preceding amino acid, established by the HN(CO)CA cross peak and/or the HNCA $C_{\alpha,i-1}$ cross peak of the same amide ^{1}H–^{15}N frequency pair, were used to search the HCACO peak table for matching $^{13}C_\alpha$ and ^{13}CO frequencies. This procedure then yields the corresponding $H_{\alpha,i-1}$ frequency or a set of possible $H_{\alpha,i-1}$ frequencies in cases where the $^{13}C_\alpha$ and ^{13}CO frequencies do not uniquely determine H_α. In the next step, the peak tables of the HNCA, ^{15}N-separated HOHAHA, and ^{15}N-separated NOESY spectra are searched simultaneously for all possible ^{15}N–^{1}H amide pairs that correlate both to $C_{\alpha,i-1}$ (HNCA) and to $H_{\alpha,i-1}$ (HOHAHA/NOESY). However, particularly because of the severe overlap in the H_α/C_α correlation, this procedure frequently yields multiple possibilities. In this respect, it is important to realize that a small increase in the uncertainty of measured peak positions gives rise to a significant increase in the number of possible connectivities from which the correct one must be selected.

As is clear from the 3D NOESY spectrum and from other biophysical measurements, IFN-γ is highly helical in nature and consequently its NOESY spectrum shows a large number of d_{NN} connectivities. These d_{NN} connectivities were used to resolve the ambiguities remaining whenever the above search procedure yielded multiple possibilities for (H_α, H_N, and $N)_{i-1}$. This matching of intraresidue connectivities is described most

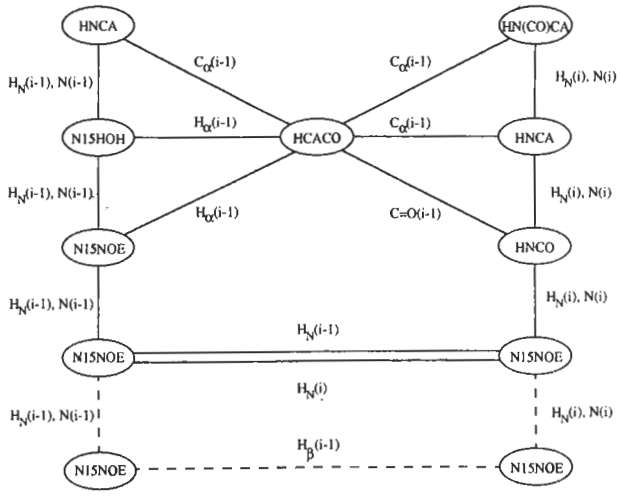

FIGURE 4: Schematic search graph for interresidue assignments. In graph theoretical terms, each node represents a single cross peak of a given experiment, and the edges represent the frequencies that different cross peaks (nodes) have in common. The problem of correlating two adjacent amino acids by backbone *J* connectivities consists of looking through all the peak tables of the different experiments and finding the set of cross peaks that fullfills the frequency relationships defined in the graph. The connections shown by the dashed lines were not used in the computerized search but were used instead for conformation of the interresidue assignment after the number of possible choices had been narrowed down to 1 or 2.

naturally in graph-theoretical terms [e.g., Christofides (1975)]. Figure 4 shows such a graph for the search procedure described above. The nodes of the graph represent the matching cross peaks from the various experimental peak tables, and the edges of the graph represent the frequencies by which these cross peaks are related. The backbone assignment problem consists of finding the unique graphs for all interresidual connections. For a different protein, a different set of experiments and therefore a different connecting graph may be more useful. A program has been developed which performs this type of graph matching for any given number of peak tables and any given type of connecting graph. Table I illustrates data extracted by the program from the pertinent peak tables for making the E10–N11 connectivity.

The complete set of backbone assignments for Q2 to Q134, determined in the manner described above, is presented in Table II.

Secondary Structure Results. Once a complete assignment of the ^1H–^{15}N correlations is available, intraresidue and sequential NOEs involving these amide protons are very easily visualized by cutting the corresponding "strips" through the 3D ^{15}N-separated NOESY spectrum (Marion et al., 1989a). Figure 5A shows such a "strip plot" for the amino acid stretch from N11 to S21. The fact that some of the strongest cross peaks are only about 3-fold weaker than the diagonal peak of the amide proton (when not subject to fast solvent exchange) indicates that spin diffusion must be extensive at the 70-ms mixing period used. However, both the number of NOE cross peaks and their relative intensities are comparable with those observed for other somewhat smaller proteins with longer NOE mixing times (Wüthrich et al., 1991; Borden et al., 1992; Marion et al., 1989a), and this degree of spin diffusion does not prohibit determination of secondary structure. For example, the stretch of d_{NN} NOE connectivities from E10 through G19 observed in Figure 5A (marked by dotted lines) contains part of the first α-helix. The absence of d_{NN} connectivities between G19, H20, S21, and D22 marks the beginning of the first interhelical loop region. Intraresidue

Table I: Example of Peak Positions Measured from the 3D Spectra That Were Used for Determining the Glu-10 to Asn-11 Sequential Assignment

	H_N (10)	^{15}N (10)	H_α (10)	$^{13}C_\alpha$ (10)	$^{13}C{=}O$ (10)	H_N (11)	^{15}N (11)
HNCA	8.320	118.98		59.49			
N15HOH	8.324	118.96	4.101				
N15NOE	8.312	119.01	4.086				
N15NOE	8.332	119.02				7.946	
HCACO			4.081	59.39	179.84		
HNCO					179.65	7.940	119.57
HN(CO)CA				59.59		7.950	119.69
N15NOE	8.326					7.942	119.58

NOE H_N–H_α cross peaks have been marked by asterisks in Figure 5A. However, the high degree of H_α chemical shift degeneracy makes it difficult or impossible to extract unambiguous H_N–H_α NOE information from the ^{15}N-separated 3D NOESY. Instead, results from the 4D $^{13}C/^{15}N$-separated NOESY were used for this purpose. Figure 5 panels B and C show generalizations of the strip plot for the 4D case and illustrate the amide to aliphatic NOEs observed for K14 and N17. The strips taken through the 4D spectrum disperse the NOE cross peaks into a fourth dimension, corresponding to the chemical shift of the ^{13}C attached to the aliphatic protons. Analysis of sequential $d_{\alpha N}$ NOE connectivities is quite straightforward when comparing such "strip planes" for neighboring amino acids. For example, the strip plane of K14 (Figure 5B) shows the NOEs of its amide proton to its intraresidue H_α, as well as to the H_α of K13 and N11. In a similar way, Figure 5C depicts the connectivities for the N17 H_N resonance to the H_α of N17, F16, and K14 as well as to G19 (NOE connectivities to protons other than H_α have not yet been assigned). Clearly, the NOE connectivities are much better resolved in the 4D spectrum (Figure 5B,C) than in the 3D spectrum. However, it should be mentioned that the sensitivity of the 4D experiment is substantially lower compared to the 3D experiment, primarily because the decay of magnetization during the ^1H–^{13}C HMQC step of the experiment is not negligible for proteins as large as IFN-γ. It is also interesting to note that the resolution in the aliphatic ^1H dimension is lower in the 4D case compared to the 3D experiment, because for the 4D case the ^{13}C labeling of the protein causes an approximate doubling of the aliphatic proton line widths compared to the ^{12}C protein, used in the 3D experiment (Ikura et al., 1990b).

Figure 6 summarizes the sequential NOE connectivities that have been extracted from the 3D and 4D NOESY spectra and also provides qualitative information on the amide proton exchange data. Furthermore, deviations from the random coil values of the $^{13}C_\alpha$ and $^{13}C_\beta$ chemical shifts, which also correlate with secondary structure (Spera & Bax, 1991), are included in this figure. All the $d_{\alpha N}(i,i+n)$ connectivities shown in this figure have been derived from the analysis of the 4D NOESY.

The first helix, A, starts from P4 and ends at N17, judged by the simultaneous presence of consecutive $d_{NN}(i,i+1)$ connectivities, weak sequential $d_{\alpha N}$ connectivities, and a contiguous set of large positive C_α secondary shifts. Helix A appears to be α-helical as judged from the presence of many $d_{\alpha N}(i,i+3)$ NOEs, at least one $d_{\alpha N}(i,i+4)$ NOE, and the absence of $d_{\alpha N}(i,i+2)$ NOEs (Wüthrich, 1986). The exact nature of the structure at A18 through H20 is unclear at the present stage of analysis. However, a long loop, also observed in the X-ray crystal structure, extends from H20 to F30 and is largely extended as judged by the intense $d_{\alpha N}$ NOEs, largely absent

Table II: Backbone Assignment of Human IFN-γΔ10

	^{15}N	H_N	$^{13}C{=}O$	$^{13}C_\alpha$	H_α		^{15}N	H_N	$^{13}C{=}O$	$^{13}C_\alpha$	H_α
Gln-2			175.02	55.54	4.38	Ile-74	121.87	7.80	177.60	64.98	3.57
Asp-3	124.33	8.51	175.58	53.48	4.65	Lys-75	119.31	8.67	178.71	60.96	3.87
Pro-4			178.36	65.51	4.24	Glu-76	118.51	8.00	178.57	59.11	4.31
Tyr-5	113.39	8.30	176.30	60.36	4.09	Asp-77	120.49	7.68	179.00	57.90	4.57
Val-6	122.27	7.08	177.71	66.77	3.26	Met-78	118.25	8.51	178.30	60.88	3.74
Lys-7	118.57	7.75	179.79	59.14	4.00	Asn-79	119.10	8.62	178.64	56.76	4.80
Glu-8	115.96	7.73	178.98	57.55	4.64	Val-80	121.02	8.13	179.12	66.78	3.72
Ala-9	123.27	8.63	180.89	55.73	4.06	Lys-81	116.72	8.33	177.59	59.57	3.99
Glu-10	118.99	8.33	179.75	59.49	4.09	Phe-82	115.80	8.72	175.93	59.31	4.46
Asn-11	119.58	7.94	178.21	56.40	4.55	Phe-83	110.87	7.26	175.78	57.79	4.29
Leu-12	119.52	8.20	178.50	58.25	4.18	Asn-84	117.18	7.36	174.98	54.52	4.68
Lys-13	118.99	8.20	178.74	60.74	3.90	Ser-85	106.47	8.46	172.68	59.77	3.79
Lys-14	117.99	7.84	179.05	59.38	4.12	Asn-86	119.02	7.45	175.62	52.50	4.81
Tyr-15	119.95	8.00	177.33	61.07	4.12	Lys-87	128.68	8.84	177.35	59.73	3.82
Phe-16	115.33	8.23	175.80	59.82	4.33	Lys-88	118.89	7.93	178.23	59.31	4.15
Asn-17	117.88	8.11	175.56	54.10	4.66	Lys-89	121.43	7.68	177.32	59.37	3.51
Ala-18	121.57	8.18	177.83	52.89	4.33	Arg-90	117.99	7.30	177.94	58.62	2.52
Gly-19	107.17	8.43	174.05	45.38	3.88	Asp-91	120.13	8.69	179.67	57.56	4.31
His-20	120.86	8.19	176.31	56.33	4.37	Asp-92	123.21	8.48	177.57	58.02	4.48
Ser-21	123.18	8.40	174.14	58.53	4.36	Phe-93	119.41	7.78	177.48	62.33	4.00
Asp-22	122.50	8.55	176.47	54.53	4.60	Glu-94	118.69	8.81	179.18	59.67	3.87
Val-23	119.23	7.91	175.86	62.48	4.02	Lys-95	120.04	7.96	178.76	59.80	3.72
Ala-24	125.89	8.19	177.33	52.56	4.22	Leu-96	115.06	7.42	179.77	57.32	3.54
Asp-25	119.01	8.00	175.96	54.18	4.55	Thr-97	106.24	7.64	175.29	63.58	4.01
Asn-26	118.83	8.31	175.88	53.20	4.68	Asn-98	117.81	7.19	176.16	53.40	4.84
Gly-27	109.00	8.32	174.12	45.30	3.99	Tyr-99	119.82	6.88	176.63	56.64	4.78
Thr-28	110.97	8.01	174.62	60.37	4.46	Ser-100	117.25	8.77	175.64	56.67	4.81
Leu-29	126.93	11.50	179.58	55.77	4.00	Val-101	122.32	8.42	175.56	63.11	3.95
Phe-30	120.18	10.68	178.17	56.82	5.02	Thr-102	106.85	7.66	174.13	61.64	4.13
Leu-31	117.28	7.78	178.99	58.73	3.92	Asp-103	123.38	7.16	176.76	53.63	4.70
Gly-32	106.60	8.06	175.82	46.98	3.66	Leu-104	128.82	8.89	179.10	58.50	4.01
Ile-33	122.30	7.48	178.55	64.92	3.89	Asn-105	116.33	8.41	178.17	56.58	4.47
Leu-34	117.10	7.99	178.43	58.08	4.12	Val-106	122.38	7.67	177.87	66.47	3.34
Lys-35	115.43	7.48	177.38	57.76	4.11	Gln-107	117.46	8.49	177.88	60.33	3.65
Asn-36	115.29	7.35	175.03	54.05	4.13	Arg-108	115.45	7.95	179.22	60.54	3.71
Trp-37	118.57	6.86	174.17	55.50	5.01	Lys-109	119.39	7.76	178.12	60.11	4.01
Lys-38	122.80	8.40	177.59	56.93	4.47	Ala-110	120.20	8.76	182.24	55.07	3.88
Glu-39	121.30	9.19	178.38	56.71	4.37	Ile-111	120.70	8.38	177.71	62.98	4.03
Glu-40	126.04	9.01	178.14	60.12	4.12	His-112	121.41	8.48	178.06	60.94	4.22
Ser-41	113.23	8.95	175.55	62.92	3.90	Glu-113	116.55	8.19	175.91	58.24	4.27
Asp-42	118.91	6.75	178.05	58.15	4.22	Leu-114	120.05	7.16	177.35	59.48	3.99
Arg-43	118.45	8.58	179.41	61.04	3.70	Ile-115	117.62	8.64	178.31	66.30	3.66
Lys-44	118.70	8.68	179.73	58.88	4.26	Gln-116	119.39	8.02	179.20	59.12	4.15
Ile-45	117.61	7.64	179.11	67.80	3.73	Val-117	121.23	8.68	178.18	67.31	3.27
Met-46	115.45	7.31	179.37	56.28	4.29	Met-118	116.53	8.40	179.06	58.13	3.77
Gln-47	117.74	9.78	177.32	58.80	3.53	Ala-119	120.21	7.40	179.84	54.63	4.16
Ser-48	109.17	8.23	176.81	61.30	4.37	Glu-120	116.14	7.60	176.83	56.48	4.31
Gln-49	112.10	6.66	178.24	56.70	4.06	Leu-121	116.27	7.30	176.62	55.80	4.15
Ile-50	122.34	7.59	176.61	65.26	3.10	Ser-122	112.76	7.34	172.64	57.19	4.64
Val-51	119.01	8.46	177.50	67.62	3.25	Pro-123			176.82	63.41	4.51
Ser-52	111.58	7.99	176.94	62.17	4.05	Ala-124	125.26	8.48	177.80	52.58	4.26
Phe-53	124.08	7.74	177.12	62.71	4.01	Ala-125	123.22	8.31	178.05	52.55	4.31
Tyr-54	117.99	8.25	177.30	64.03	3.56	Lys-126	120.58	8.39	177.02	56.45	4.40
Phe-55	117.16	8.79	179.75	59.56	4.39	Thr-127	114.10	8.10	175.16	61.93	4.38
Lys-56	121.13	8.00	178.80	59.91	3.96	Gly-128	110.84	8.41	174.07	45.38	4.00
Leu-57	123.29	8.39	179.11	58.41	3.61	Lys-129	118.49	8.06	175.65	56.43	4.30
Phe-58	114.98	8.78	179.27	57.15	4.47	Arg-130	127.62	7.99	176.31	56.30	4.16
Lys-59	119.89	7.70	178.25	59.25	4.11	Lys-131	117.51	8.39	176.52	56.45	4.30
Asn-60	116.72	7.68	175.99	55.00	4.50	Arg-132	122.78	8.45	176.58	56.28	4.27
Phe-61	117.60	7.53	176.31	56.87	4.96	Ser-133	123.13	8.38	173.56	58.53	4.44
Lys-62	118.94	7.54	176.12	58.39	4.16	Gln-134	126.35	8.00	180.54	57.66	4.18
Asp-63	117.29	8.31	175.56	54.87	4.69						
Asp-64	120.40	7.63	176.74	53.80	4.72	Ser-21*				58.42	
Gln-65	125.27	8.90	178.09	58.89	4.00	Asp-22*	122.37	8.49	176.32	54.47	4.59
Ser-66	114.89	8.61	176.05	61.58	4.26	Val-23*	119.38	7.98	175.52	62.24	
Ile-67	114.46	7.21	176.69	60.69	4.42	Ala-24*	127.29	8.22	177.06	52.20	4.31
Gln-68	121.29	7.73	177.69	59.56	3.86	Ala-24**	126.79	8.25	177.12	52.61	4.17
Lys-69	119.00	8.32	179.84	59.31	3.99	Asp-25*	119.60	8.16		54.28	4.55
Ser-70	117.40	7.82	175.54	63.00	4.13						
Val-71	119.11	8.07	177.18	66.84	2.94	Lys-131*			176.74	56.36	
Glu-72	118.65	8.27	179.45	59.61	3.87	Arg-132*	122.37	8.37	175.44	56.33	4.34
Thr-73	116.14	7.86	176.45	67.09	3.95	Ser-133*	127.67	7.99	181.35	57.97	4.15

d_{NN} NOEs, and near random coil values of the secondary $^{13}C_\alpha$ and $^{13}C_\beta$ shifts. Many of the residues in this loop yield very intense correlations in the 2D ^1H–^{13}C correlation spectrum and in the 3D HCACO spectrum, indicative of narrow ^1H and ^{13}C line widths, caused by a high degree of internal flexibility. This loop also contains an *N*-glycosyla-

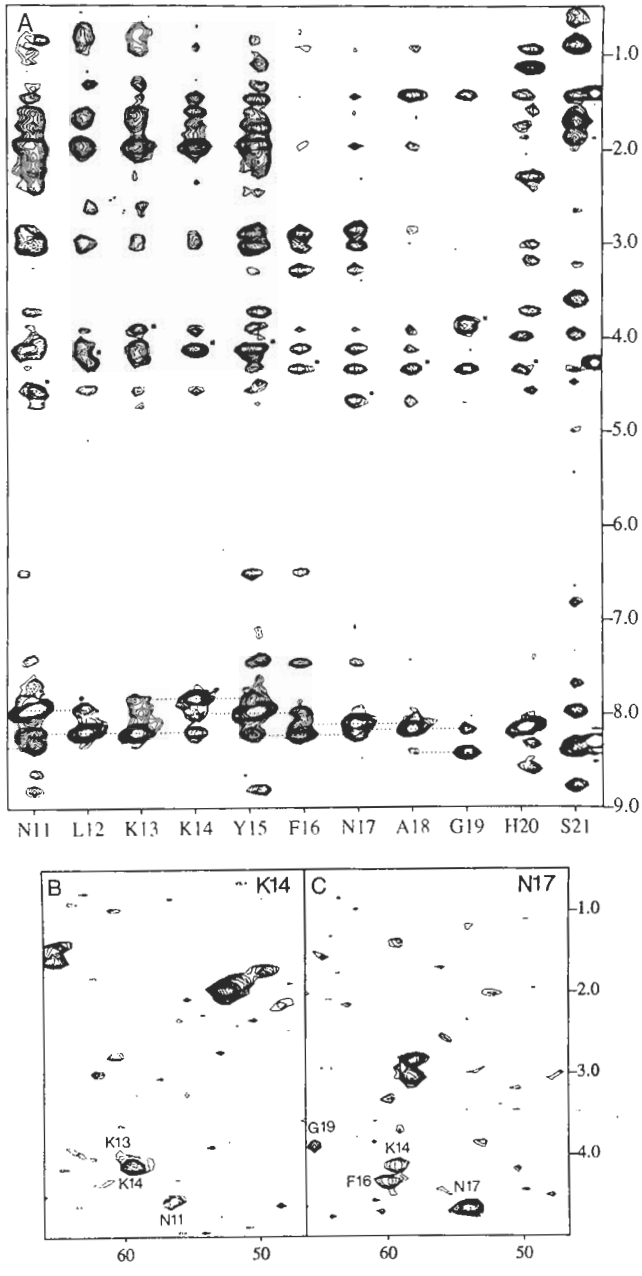

FIGURE 5: (A) Composite of NOE strips taken from the 70-ms mixing time 3D ^{15}N-separated NOESY spectrum of IFN-γ for the amides of residues N11–S21. The d_{NN} NOE connectivities have been marked by dotted lines. Intraresidue H_N–H_α NOE connectivities are marked by asterisks. (B and C) Generalizations for the 4D case of the 3D NOE strip plot in panel A. Data shown are 2D cross sections through the 60-ms mixing time 4D ^{13}C/^{15}N-separated NOESY spectrum of IFN-γ, taken at the ^1H_N (F_4) and ^{15}N (F_3) frequencies of K14 (B) and N17 (C).

tion site at N26, indicative of solvent exposure (Rinderknecht et al., 1984).

The second helix, B, is rather short and runs from L31 through N36. The NMR data indicate that this helix starts two residues later compared to the X-ray structure, primarily because the secondary C_α shifts for L29 and F30 appear incompatible with a regular helical structure, and because the d_{NN} connectivities for these residues are rather weak. In addition, no $d_{\alpha N}(i,i+3)$ connectivity is observed until residue I33.

A stretch of helical structure, labeled C, extends from E40 to F58. Helix C is found in the crystal structure at the monomer–monomer interface and is very hydrophobic in nature (Ealick et al., 1991). Amide proton exchange data indicate that many of the amides in this helix are protected from solvent exchange, indicative of strong hydrogen bonding and low solvent accessibility. From S41 through K44, d_{NN} cross peaks are relatively strong and large positive secondary shifts for C_α are observed, indicative of helical character. From K44 through S48 d_{NN} cross peaks are weaker, but so are the amide diagonal peak intensities of these residues. Starting at I45 through N60 many $d_{\alpha N}(i,i+3)$ cross peaks are observed, indicating that helix C is presumably α-helical. A single $d_{\alpha N}(i,i+2)$ and a number of $d_{NN}(i,i+2)$ connectivities in this helix are presumably caused in part by spin diffusion. Residues F58 and F61 are marked by negative secondary shifts which are highly unusual for residues in an α-helical conformation (Spera & Bax, 1991). Also, from K59 through D64 a set of $d_{\alpha N}(i,i+2)$ cross peaks is observed, together with weaker or absent $d_{\alpha N}(i,i+3)$ cross peaks and strong d_{NN} connectivities. This suggests that this region may be either a 3_{10} helix, or it may consist of several helical turns and it is probably not a regular α-helix.

There is a notable absence of d_{NN} connectivity between D64 and Q65, but from Q65 through K81 the polypeptide chain continues as an α-helix (helix D), based on numerous $d_{\alpha N}(i,i+3)$ and strong d_{NN} connectivities combined with large positive secondary C_α shifts. However, residue I67 has a negative secondary C_α shift, and it is therefore uncertain whether helix D starts at Q65 or at Q68 preceded by a helical turn.

The end of helix D is not defined very clearly by the NMR data. However, as no $d_{\alpha N}(i,i+3)$ connectivities are observed for residues F82–K87, and a decrease in secondary C_α shift is observed for these residues, helix D presumably terminates at K81. Note, however, that the amide protons of F82 and F83 exchange very slowly with solvent, suggesting that they are hydrogen bonded. Also, d_{NN} connectivities are observed for F82 and F83, whereas $d_{\alpha N}$ connectivities are absent for these two residues and it is therefore possible that these two residues are still part of helix D.

Helix E (K87–N98) is marked by relatively strong d_{NN} connectivities, a large number of $d_{\alpha N}(i,i+3)$ NOEs, and large positive secondary C_α shifts. The last two residues of the helix show smaller secondary shifts, however, and two $d_{\alpha N}(i,i+2)$ connectivities are also observed, suggesting that the ϕ,ψ angles of the last two residues may deviate from ideality. Amide exchange for a number of residues in helix E is particularly slow, indicating that this helix is resistant to local unfolding. N98 is the second site of glycosylation in natural IFN-γ (Rinderknecht et al., 1984), and the end of helix E is therefore almost certainly exposed to solvent.

The last helix, F, starts at L104 and continues through either A119 or S122. This α-helix is also marked by strong d_{NN} connectivities, a substantial number of $d_{\alpha N}(i,i+3)$ NOEs, a number of very slowly exchanging amide protons, and large secondary C_α shifts. As was the case for helices A and E, the last few residues of helix F show $d_{\alpha N}(i,i+2)$ NOEs plus secondary C_α shifts substantially smaller than expected for a regular α-helix, indicating a deviation from α-helical geometry. Near the center of helix F, a very high (6.64 ppm) C_α secondary shift for H112 together with five $d_{NN}(i,i+2)$ NOEs are observed. This anomaly coincides with the helical bend of 125° centered at E113 which has been reported in the crystal structure (Ealick et al., 1991).

Beyond P123, no further NOEs or secondary C_α or C_β shifts are observed that are indicative of a defined secondary structure. Furthermore, most of the amide protons of this C-terminal region of the protein exchange rapidly with the solvent, judged by the substantial attenuation of these

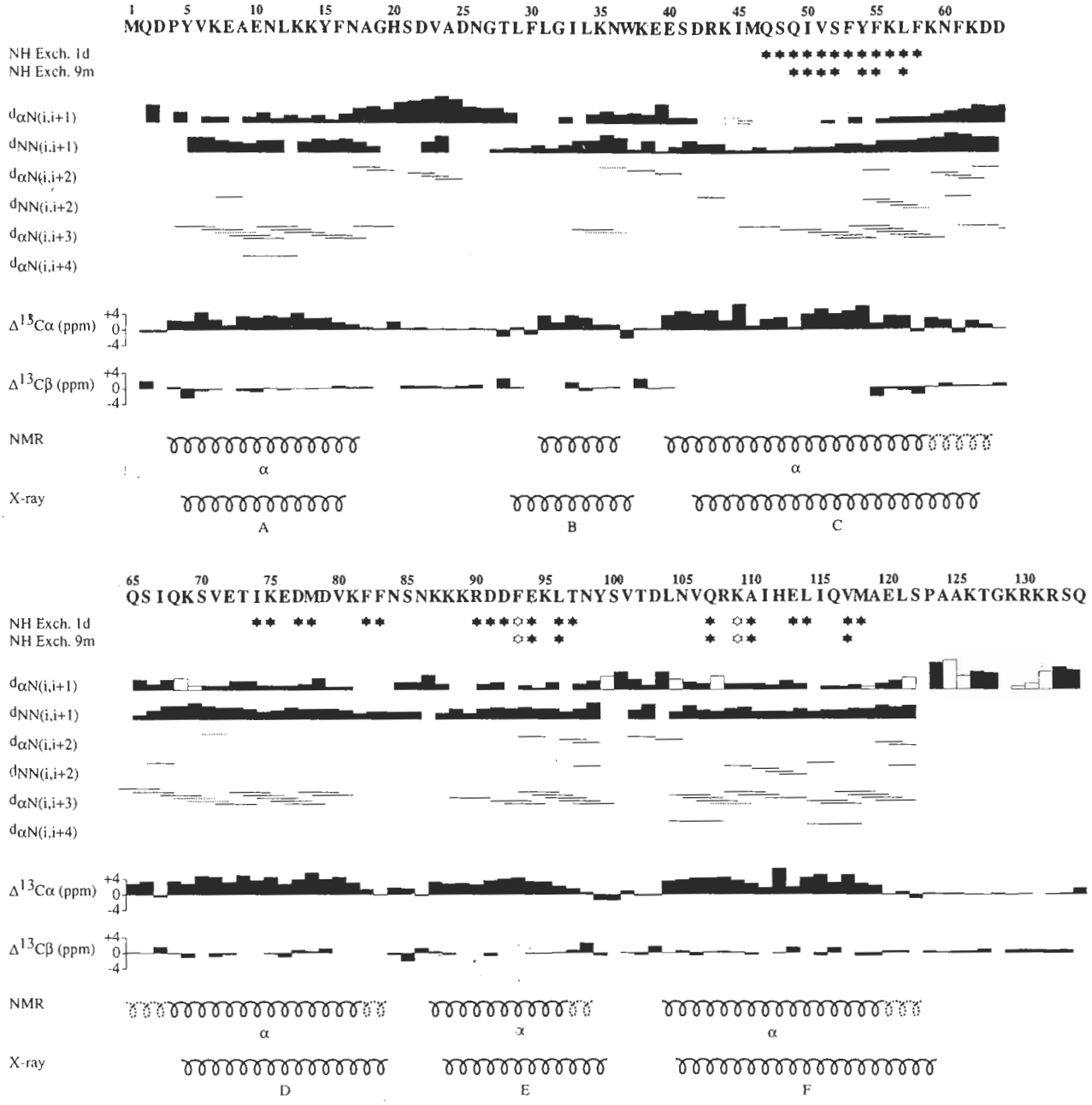

FIGURE 6: Summary of the sequential and medium-range NOEs involving the H_N and H_α protons, the amide exchange data, and the $^{13}C_\alpha$ and $^{13}C_\beta$ secondary shifts observed for IFN-$\gamma\Delta$10, together with the secondary structure deduced from these data. Helices drawn by broken lines are presumably not α-helical but consist of either 3_{10} helix or helical turns. Also shown (marked by X-ray) is the definition of the helices derived from the crystal structure (Ealick et al., 1991). Amide protons which were still present after 1 day (1d) or 9 months (9m) are marked by stars. Open stars are tentative assignments because of overlap in the 2D ^1H–^{15}N spectrum. The thickness of the lines for the $d_{\alpha N}$ and d_{NN} ($i,i+1$) connectivities corresponds to the intensities of the cross peaks. All $d_{\alpha N}$ NOE connectivities have been derived exclusively from the 4D $^{13}C/^{15}N$-separated NOESY spectrum. Connectivities that could not be assigned unambiguously because of resonance overlap are shown either as open boxes or as dotted lines.

resonances upon water presaturation. The line widths of resonances in this part of the protein are narrower by more than a factor of 2 as compared to resonances of helical residues. It is therefore concluded that, starting at P123, the functionally important C-terminus (Döbeli et al., 1988), which was not observed in the X-ray structure (Ealick et al., 1991), adopts a highly flexible conformation.

Comparison with Crystal Structures. Figure 6 also shows the helical definition of the 3.5-Å crystal structure (Ealick et al., 1991), which generally agrees quite well with our NMR observations. However, the pronounced distortion from an α-helical conformation at the end of helix C was not reported in the X-ray study. Although the overall folding topology of the crystal structures of human IFN-γ (Ealick et al., 1991) and rabbit IFN-γ (Samudzi et al., 1991) are quite similar, the definitions of the α-helical segments for these two proteins differ substantially, particularly for helices D, E, and F. The present NMR results agree much better with the helical definitions as observed in the crystal structure of human IFN-γ (3.5-Å resolution; Ealick et al., 1991) than with the rabbit IFN-γ crystal structure (2.7-Å resolution; Samudzi et al., 1991).

CONCLUSIONS

Our results obtained for interferon-γ indicate that the triple-resonance backbone assignment procedure is applicable to proteins in the 30-kDa range, despite the large resonance line widths for resonances of residues with low degrees of internal

mobility. For proteins that can be studied at temperatures higher than 27 °C or that have inherently narrower line widths, the triple-resonance procedure may be applicable to even higher molecular masses. One of the major problems, faced in our study of IFN-γ, was the presence of very intense correlations from residues with high degrees of internal mobility which frequently obliterate the very weak resonances from residues in well-defined regions of secondary structure. Preliminary results indicate that this difference in line width and resonance intensity constitutes an even more difficult problem in the analysis of the ^{13}C-separated 3D (Ikura et al., 1990b; Zuiderweg et al., 1990) or 4D (Clore et al., 1991; Zuiderweg et al., 1991) NOE spectra.

To the best of our knowledge, the present study of IFN-γ is the first case where NOE data involving amide protons and aliphatic protons are obtained primarily from a 4D NMR spectrum. In previous studies the 4D spectrum was used mainly to resolve ambiguities in the 3D spectrum. Resonance dispersion of IFN-γ is so poor that only a small fraction of the NOEs can be obtained unambiguously from the 3D spectrum whereas analysis of the 4D spectrum is much more straightforward. The NOE information involving amide protons alone, however, is frequently insufficient for accurate definition of secondary structure, particularly because, for sensitivity reasons, the NOE spectrum must be recorded with a relatively long mixing time which results in spin diffusion. Secondary C_α and C_β chemical shifts are very useful additional markers for secondary structure (Saito, 1988; Spera & Bax, 1991; Wishart et al., 1991) and are easily obtained with the triple-resonance experiments. However, until a better understanding of the relation between secondary shift and protein structure has been developed, these chemical shift data can only be interpreted in a very qualitative manner.

Our NMR results indicate that the secondary structure of IFN-γΔ10 in solution does not deviate significantly from that in the crystalline form. Although this result might have been anticipated on the basis of previous comparisons between the solution and crystal structures of other globular proteins, it was less certain in the present case considering the low resolution of the crystal structure (3.5 Å and an *R* factor of 25%; Ealick et al., 1991). Also, the secondary structure of rabbit IFN-γ, which had been solved at 2.7 Å, differs from human IFN-γ more than expected on the basis of its high degree of sequence homology (69%) (Samudzi et al., 1991).

ACKNOWLEDGMENT

We thank W. Vetter and W. Meister for mass spectrometry measurements, P. Jakob for skillful help in protein purification, M. Zulauf for quasielastic light scattering analysis, and W. Klaus for the initial NMR characterization of IFN-γ. S.G. acknowledges funding by the ROCHE Research Foundation. Upon completion of our NMR study, M. Carson and C. E. Bugg kindly provided us with secondary structure information derived from a higher resolution crystal structure of human IFN-γ (unpublished) which appears in very good agreement with our NMR results.

REFERENCES

Arakawa, T., Hsu, Y.-R., Parker, C. G., & Lai, P.-H. (1986) *J. Biol. Chem. 261*, 8534–8539.

Arakawa, T., Hsu, Y.-R., & Yphantis, D. A. (1987) *Biochemistry 26*, 5428–5432.

Bax, A., Ikura, M., Kay, L. E., Torchia, D. A., & Tschudin, R. (1990) *J. Magn. Reson. 86*, 304–318.

Bodenhausen, G., & Ruben, D. J. (1980) *Chem. Phys. Lett. 69*, 185–188.

Borden, K. L. B., Bauer, C. J., Frenkiel, T. A., Beckmann, P., & Lane, A. N. (1992) *Eur. J. Biochem. 204*, 137–146.

Boucher, W., Laue, E. D., Campbell-Burk, S., & Domaille, P. J. (1992) *J. Am. Chem. Soc. 114*, 2262–2264.

Certa, U., Banwarth, W., Stüber, D., Gentz, R., Lanzer, M., Le Grice, S., Guillot, F., Wendler, J., Hunsmann, G., Bujard, H., & Mous, J. (1986) *EMBO J. 5*, 3051–3056.

Christofides, N. (1975) *Graph Theory*, Academic Press, New York.

Clore, G. M., Kay, L. E., Bax, A., & Gronenborn, A. M. (1991) *Biochemistry 30*, 12–18.

Clubb, R. T., Thanabal, V., & Wagner, G. (1992) *J. Magn. Reson. 97*, 213–217.

Curling, E. M. A., Hayter, P. M., Baines, A. J., Bull, A. T., Gull, K., Strange, P. G., & Jenkins, N. (1990) *Biochem. J. 272*, 333–337.

De la Maza, L. M., Peterson, E. M., Burton, L. E., Gray, P. W., Rinderknecht, E., & Czarniecki, C. W. (1987) *Infect. Immun. 55*, 2727–2733.

Döbeli, H., Gentz, R., Jucker, W., Garotta, G., Hartmann, D. W., & Hochuli, E. (1988) *J. Biotechnol. 7*, 199–216.

Ealick, S. E., Cook, W. J., Vijay-Kumar, S., Carson, M., Nagabhushan, T. L., Trotta, P. P., & Bugg, C. E. (1991) *Science 252*, 698–702.

Garrett, D. S., Powers, R., Gronenborn, A. M., & Clore, G. M. (1991) *J. Magn. Reson. 95*, 214–220.

Grzesiek, S., & Bax, A. (1992a) *J. Magn. Reson. 96*, 432–440.

Grzesiek, S., & Bax, A. (1992b) *J. Am. Chem. Soc.* (in press).

Hogrefe, H. H., McPhie, P., Bekisz, J. B., Enterline, J. C., Dyer, D., Webb, D. S. A., Gerrard, T. L., & Zoon, K. (1989) *J. Biol. Chem. 264*, 12179–12186.

Ijzermans, J. N. M., & Marquet, R. L. (1989) *Immunobiol. 179*, 456–473.

Ikura, M., Kay, L. E., & Bax, A. (1990a) *Biochemistry 29*, 4659–4667.

Ikura, M., Kay, L. E., Tschudin, R., & Bax, A. (1990b) *J. Magn. Reson. 86*, 204–209.

Ikura, M., Kay, L. E., & Bax, A. (1991) *J. Biomol. NMR 1*, 299–304.

Isaacs, A., & Lindenmann, J. (1957) *Proc. R. Soc. London, B 147*, 258–267.

Jarpe, M. A., & Johnson, H. M. (1990) *J. Immunol. 145*, 3304–3309.

Johnson, H. M., Langford, M. P., Lakhchaura, B., Chan, T.-S., & Stanton, G. J. (1982) *J. Immunol. 129*, 2357–2359.

Kay, L. E., Marion, D., & Bax, A. (1989) *J. Magn. Reson. 84*, 72–84.

Kay, L. E., Clore, G. M., Bax, A., & Gronenborn, A. M. (1990a) *Science 249*, 411–414.

Kay, L. E., Ikura, M., Tschudin, R., & Bax, A. (1990b) *J. Mag. Reson. 89*, 496–514.

Kay, L. E., Ikura, M., Zhu, G., & Bax, A. (1991) *J. Magn. Reson. 91*, 422–428.

Landolfo, S., & Garotta, G. (1991) *J. Immunol. Res. 3*, 481–494.

Langer, J. A., & Pestka, S. (1988) *Immunol. Today 9*, 393–400.

Le, J., Barrowclough, B. S., & Vilcek, J. (1984) *J. Immunol. Methods 69*, 61–70.

Lortat-Jacob, H., & Grimaud, J.-A. (1991) *Cell. Mol. Biol. 37*, 253–260.

Marion, D., Driscoll, P. C., Kay, L. E., Wingfield, P. T., Bax, A., Gronenborn, A. M., & Clore, G. M. (1989a) *Biochemistry 28*, 6150–6156.

Marion, D., Ikura, M., Tschudin, R., & Bax, A. (1989b) *J. Magn. Reson. 85*, 393–399.

Marion, D., Kay, L. E., Sparks, S. W., Torchia, D. A., & Bax, A. (1989c) *J. Am. Chem. Soc. 111*, 1515–1517.

Messerle, B. A., Wider, G., Otting, G., Weber, C., & Wüthrich, K. (1989) *J. Magn. Reson. 85*, 608–613.

Mosmann, T. R., Schumacher, J. H., Street, N. F., Budd, R., O'Garra, A., Fong, T. A. T., Bond, M. W., Moore, K. W. M., Sher, A., & Fiorentino, D. F. (1991) *Immunol. Rev. 123*, 209–229.

Murray, H. W. (1990) *Diagn. Microbiol. Infect. Dis. 13*, 411–421.

Nathan, I., Groopman, J. E., Quan, S. G., Bersch, N., & Golde, D. W. (1981) *Nature 292*, 842–844.

Pan, Y.-C. E., Stern, A. S., Familetti, P. C., Khan, F. R., & Chizzonite, R. (1987) *Eur. J. Biochem. 166*, 145–149.

Pestka, S., Kelder, B., Familletti, P. C., Moschera, J. A., Crowl, R., & Kempner, E. S. (1983) *J. Biol. Chem. 258*, 9706–9709.

Powers, R., Gronenborn, A. M., Clore, G. M., & Bax, A. (1991) *J. Magn. Reson. 94*, 209–213.

Rinderknecht, E., O'Connor, B. H., & Rodriguez, H. (1984) *J. Biol. Chem. 259*, 6790–6797.

Saito, H. (1986) *Magn. Reson. Chem. 24*, 835–852.

Samudzi, C. T., Burton, L. E., & Rubin, J. R. (1991) *J. Biol. Chem. 266*, 21791–21797.

Seelig, G. F., Wijdenes, J., Nagabhushan, T. L., & Trotta, P. P. (1988) *Biochemistry 27*, 1981–1987.

Shaka, A. J., Lee, C. J., & Pines, A. (1988) *J. Magn. Reson. 77*, 274–293.

Shows, T. B., Sakaguchi, A. Y., Naylor, S. L., Goeddel, D. V., & Lawn, R. M. (1982) *Science 218*, 373–374.

Sklenar, V., & Bax, A. (1987a) *J. Magn. Reson. 74*, 469–479.

Sklenar, V., & Bax, A. (1987b) *J. Magn. Reson. 75*, 478–383.

Spera, S., & Bax, A. (1991) *J. Am. Chem. Soc. 113*, 5490–5492.

Trinchieri, G., Matsumoto-Kobayashi, M., Clark, S. V., Sheera, J., London, L., & Perussia, B. (1984) *J. Exp. Med. 160*, 1147–1169.

Wheelock, E. F. (1965) *Science 149*, 310–311.

Wishart, D. S., Sykes, B. D., & Richards, F. M. (1991) *J. Mol. Biol. 222*, 311–333.

Wüthrich, K. (1986) *NMR of Proteins and Nucleic Acids*, Wiley, New York.

Wüthrich, K., Spitzfaden, C., Memmert, K., Widmer, H., & Wider, G. (1991) *FEBS Lett. 285*, 237–247.

Zhu, G., & Bax, A. (1990) *J. Magn. Reson. 90*, 405–410.

Zuiderweg, E. R. P., & Fesik, S. W. (1989) *Biochemistry 28*, 2387–2391.

Zuiderweg, E. R. P., McIntosh, L. P., Dahlquist, F. W., & Fesik, S. W. (1990) *J. Magn. Reson. 86*, 210–216.

Zuiderweg, E. R. P., Petros, A. M., Fesik, S. W., & Olejniczak, E. T. (1991) *J. Am. Chem. Soc. 113*, 370–372.